

Experimental study of separation of magnetization precession in $^3\text{He-B}$ into two magnetic domains

A. S. Borovik-Romanov, Yu. M. Bun'kov, V. V. Dmitriev, Yu. M. Mukharskiĭ, and K. Flachbart¹⁾

Institute of Physical Problems, Academy of Sciences of the USSR

(Submitted 15 February 1985)

Zh. Eksp. Teor. Fiz. **88**, 2025–2038 (June 1985)

The precession of the nuclear spin magnetization in $^3\text{He-B}$ after excitation by an rf pulse in a nonuniform static magnetic field is found to split into two homogeneous magnetic domains. The spatial precession of the magnetization is uniform in one domain and at rest in the other. The splitting is caused by spin supercurrents which carry the longitudinal magnetization toward higher magnetic fields and tip (rotate) the magnetization through an angle $\sim 104^\circ$ in the region where the field is weaker. The NMR frequency shift (which is of dipole origin) compensates the formation and relaxation of the dynamic domain in which the magnetization precesses uniformly in space.

INTRODUCTION

In the 12 years since superfluid ^3He was discovered in 1972, intensive NMR studies have revealed the structure of the order parameter in superfluid ^3He and have also shed light on the interactions among the excited quasiparticles and on the extremely complicated nonlinear spin dynamics of the superfluid phases. Almost all of the NMR properties of ^3He found so far are in close agreement with theoretical predictions. For example, the frequency ω of the free-induction decay signal in He-B was found to be equal to the Larmor frequency ω_L for magnetization vectors \mathbf{M} making an angle β less than $\theta_0 = \cos^{-1}(-1/4) \sim 104^\circ$ with the applied field, and ω increases with the tipping angle β as described by the equation

$$\delta\omega(\beta) = -\frac{4}{15} \frac{\Omega_B^2}{\omega_L} (1 + 4 \cos \beta). \quad (1)$$

Here $\delta\omega(\beta)$ is the shift relative to the Larmor frequency ω_L , and $\Omega_B \sim 100$ kHz is the longitudinal resonance frequency in He-B (see Refs. 1 and 2 for experimental and theoretical work, respectively).

However, unexpected results have turned up in several experiments. For example, the magnetic relaxation process in superfluid He-B is very sensitive to the magnetic field gradient.¹ Moreover, the NMR signal was found^{3,4} to have a low-intensity "tail" ($\sim 10\%$ of the initial signal amplitude) which decayed an order of magnitude more slowly than expected from the obtained non-uniformity of the external magnetic field.

In preliminary experiments described in Ref. 5, we recorded an intense slowly decaying induction signal (SDS) of intensity as high as 95% of the initial value. The SDS was found not to be a local effect formed by all of the ^3He within the experimental chamber. The SDS was also observed for steep magnetic field gradients up to 20 Oe/cm, and the gradients increased by three decades the ratio of the duration of the SDS signal to the decay time of the free-induction signal measured in the normal ^3He phase. The persistence of the SDS in magnetic field gradients of this magnitude indicates

that these signals cannot be attributed to elasticity of the order parameter, since theoretical estimates⁶ show that elasticity can maintain a spatially uniform precession of the magnetization in $^3\text{He-B}$ only for a magnetic field gradient $|\nabla H| \lesssim \sim 10^{-5}$ Oe/cm. We have also pointed out previously⁵ that the frequency of the SDS in $^3\text{He-B}$ at $|\nabla H|$ decreases continuously with time at a rate that increases with $|\nabla H|$. Our experiments thus indicate that a macroscopic quantum effect alter the precession in $^3\text{He-B}$ throughout the experimental chamber and is responsible for the slowly decaying signal.

In work carried out while our experiments were in progress, I. A. Fomin succeeded in developing a theory that accounts for the generation and relaxation of the SDS. The preliminary theoretical results were reported in Ref. 6, and the full theory is presented following this paper in the current issue of JETP (Ref. 7). According to Ref. 6, the formation of an unusual two-domain state in $^3\text{He-B}$ is responsible for the SDS.

We tested Fomin's theoretical model experimentally by observing the splitting of the magnetization precession into two magnetic domains in a chamber equipped with two receiving NMR coils. The preliminary experimental findings, reported in Ref. 5, fully support Fomin's theory. We will describe these experiments in more detail in the present paper and briefly analyze how dissipation causes the two-domain structure to disappear.

EXPERIMENTAL SETUP

The experiments were carried out in a demagnetizing cryostat,^{8,9} which we used to demagnetize copper nuclei in a ^3He cell at temperatures as low as $420 \mu\text{K}$. The experimental chambers were attached to the demagnetizer by means of a conical junction, and both chambers had copper bases. A sintered powdered-silver heat exchanger with grain diameter $\sim 1000 \text{ \AA}$ filled the bottoms of the chambers. The upper portions of the chambers were poured from Stycast-1266 epoxy resin and were used in the pulsed NMR experiments. Figure

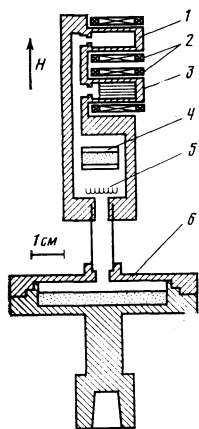


FIG. 1. Sketch of experimental chamber No. 1: 1, 3) cells used for the NMR experiments in ^3He ; 2) NMR coils; 4) PLM-3 temperature sensor; 5) heater; 6) chamber with sintered silver heat exchanger.

1 shows a sketch of chamber No. 1, which was equipped with two experimental cells; the chamber housing the PLM-3 platinum temperature sensor is also shown. The upper experimental cell was a 13-mm-long cylinder of inner diameter 5 mm and wall thickness 1.5 mm. The bottom cell was a rectangular parallelepiped which measured $4 \times 4 \times 12$ mm and was filled by a stack of 11 equally spaced lavsan films of thickness $12 \mu\text{m}$; the planes of the films were oriented normal to the external magnetic field. Both experimental cells were connected to the rest of the chamber by 4-mm-long channels of diameter 2 mm.

The receiving/transmitting NMR coils were designed prior to the experiments by using a computer. In order to avoid heating the ^3He , the coils were wound on separate thin forms and mounted on graphite supports to avoid contact with the experimental chamber. Three copper wires of diameter 0.5 mm provided the thermal contact between the NMR coils and the chamber of a separate ^3He - ^4He dissolution cryostat. Both coils were identical and consisted of 260 turns of 0.06-mm-diameter PÉL wire wound in three sections. The radio frequency (rf) field near the center of the ^3He cells was spatially uniform to within 1% (the distribution of the rf field in the chamber is described in Ref. 9).

Figure 2 shows the upper part of chamber No. 2, which was used in the main series of experiments on the splitting of the magnetization precession into two dynamic domains. The rest of chamber No. 2 is also shown, except for the heat exchanger, which was the same as in chamber No. 1. The experimental cell in chamber No. 2 was a cylinder of inner diameter 4 mm and length 8 mm and was connected to the rest of the chamber by a long, narrow channel (length 5 mm, diameter 1 mm). The constant external magnetic field was parallel to the axis of the cell. Three NMR coils were used. Coil 1 (Fig. 2) was used to tip the nuclear magnetization vector; it produced an rf field that was uniform to within 1% over the entire volume of the cell and consisted of 130 turns of 0.06-mm-diameter PÉL wire. The other two coils 2 and 3 were saddle-shaped and had identical properties; they served as the receiving coils for the pulse NMR spectrometer and consisted of 280 turns of 0.042-mm-diameter PÉL wire. The

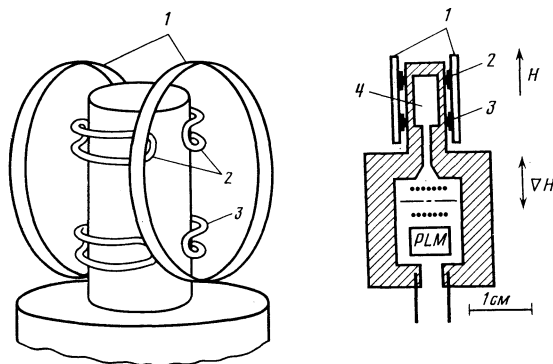


FIG. 2. Top part of NMR cell (left) and sketch of chamber No. 2 (right). 1) NMR excitation coil; 2, 3) receiving NMR coils; 4) chamber containing ^3He sample.

overlap of the sensitive regions of coils 2 and 3 was virtually nil, i.e., they recorded the induced signal from two disjoint regions of the experimental chamber (cf. Fig. 3). All three coils were mounted on graphite supports and were in thermal contact with the chamber of the dissolution cryostat. A superconducting solenoid located outside the vacuum jacket of the demagnetizing cryostat generated a constant magnetic field in the chambers. We used gradient coils (also located outside the vacuum jacket) to compensate the residual gradients and to generate a calibrated magnetic field gradient. Analysis of the decay of the induction signal in normal ^3He revealed that under optimum conditions the magnetic field was constant to within $\sim 10^{-2}$ Oe over distances comparable to the cell diameter D . In addition, calculations indicated that the gradient coils produced a field gradient that was constant to within 1% over distances $\sim D$. We used the NMR pulse spectrometer described in Ref. 9 to observe the magnetic signal in ^3He - B . An rf pulse at the resonant frequency of the rf coil was applied to tip the magnetization of the ^3He - B in the experimental cell by an angle β relative to the cell axis. The rf pulses generally contained 10 periods at $f = 500$ kHz and 4 periods at $f = 250$ kHz, and the spectral pulse width was ~ 50 kHz. We varied β by changing the amplitude $A \leq 16$ Oe of the rf tipping pulse. The precessing magnetization induced a signal in the receiving rf coil which was amplified by a broadband amplifier and stored by a Datalab-905 digital recorder. The signal was then analyzed by computer and the time dependence of the signal frequency and amplitude was calculated.

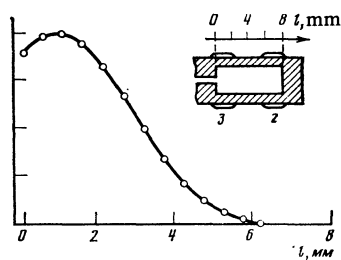


FIG. 3. Relative sensitivity of coil 3 as a function of the coordinate l of the experimental cell (the results were measured using a loop probe).

EXPERIMENTS USING CHAMBER No. 1

The pulsed NMR experiments in ${}^3\text{He-B}$ were carried out at pressures 0, 11, 20, and 29.3 bar for magnetic fields from 77 to 262 Oe (corresponding to NMR frequencies 250–850 kHz). In all cases we observed a slowly decaying signal (SDS) for temperatures away from T_c (usually, $T < 0.9T_c$ sufficed); the intensity of the SDS decayed much more slowly than predicted from the magnitude of the magnetic field gradients. For large tipping angles $\beta \sim 90\text{--}120^\circ$ the SDS intensity was as high as 80–95% of the initial signal strength. Our previous paper (Ref. 5) shows the envelope of an SDS recorded for the smallest possible $|\nabla H|$ using our equipment (the relative fluctuation was approximately 1 part per 20,000 over the length of the chamber). The SDS ($\tau = 0.5$ s) was an order of magnitude longer than the NMR signal observed from normal-phase ${}^3\text{He}$ under the same conditions.

In the absence of a magnetic field gradient. The SDS signals were weaker and their form could not be reproduced reliably for temperatures $T < 0.7T_c$ even when the experimental conditions were unchanged. However, the application of a weak gradient field stabilized the signals, which recovered their full intensity.

The NMR signal in ${}^3\text{He-B}$ can be split into two parts. Initially, the signal intensity I increases roughly in proportion to $|\nabla H|$. The decay in I then slows abruptly (I may even increase), and an SDS forms (Fig. 4). SDS formation is often accompanied by oscillations of the signal amplitude and frequency during the initial stage. The NMR signal is dephased in the initial region, which becomes narrower as $|\nabla H|$ increases. The duration τ_{SDS} of the SDS also decreases, but at a much slower rate than τ_{normal} for the normal phase of ${}^3\text{He}$. As a result, the ratio $\tau_{\text{SDS}}/\tau_{\text{normal}}$ reaches $\sim 10^{-3}$ for gradients ~ 10 Oe/cm. The amplitude I of the SDS also depends strongly on the magnitude E_{ex} of the rf excitation pulse. No SDS is observed for weak rf fields corresponding to $\beta \lesssim 30^\circ$. As E_{ex} increases, I rises to a maximum at $\beta \sim 104^\circ$ (Fig. 4). For large β , the signal frequency ω was initially shifted relative to the Larmor frequency as described by (1). A “bulk” relaxation mechanism in fact occurs in ${}^3\text{He-B}$ for $\beta > 104^\circ$ and tends to restore β to 104° . The succeeding magnitude of the SDS signal was usually the same as when the initial tipping angle was $\beta \sim 104^\circ$. No SDS signal was generated for $\beta \approx 130^\circ$.

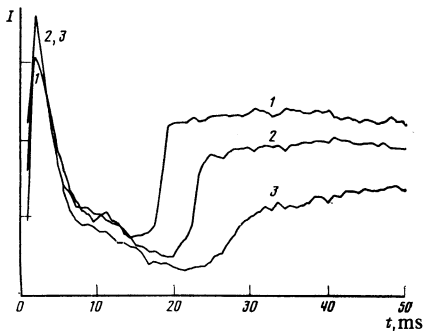


FIG. 4. Envelope of the initial portion of the induction signal in ${}^3\text{He-B}$ for initial tipping angles $\beta_0 = 105^\circ$ (1), 97° (2), and 86° (3); $H = 77$ Oe, $P = 29.3$ bar (chamber No. 1).

In the presence of a constant gradient (linear magnetic field), the SDS frequency ω decreased continuously but always remained within the range of Larmor frequencies corresponding to the range of field variation in the experimental chamber. SDS beat signals from each layer of helium were observed from the chamber containing stacked lavsan films, and the SDS frequency reflected the local field variations in each layer. Figure 5 shows a trace of the SDS signal recorded from the stack together with the Fourier transform of the signal. Twelve NMR lines are clearly discernible; each corresponds to the SDS signal from one of the ${}^3\text{He-B}$ layers in the stack. The Fourier transform of the signal from normal-phase ${}^3\text{He}$ was smooth, because the thickness of the ${}^3\text{He}$ layer between the films was 30 times greater than the film thickness.

EXPERIMENTS IN CHAMBER No. 2

We have already noted in the Introduction that the above experimental findings stimulated the development of a theory^{6,7} which describes the splitting of the magnetization precession in ${}^3\text{He-B}$ into two homogeneous magnetic domains. According to this theory, a magnetic field gradient causes the magnetization \mathbf{M} to precess; this in turn induces a gradient of the precession phase and generates a spin supercurrent. The supercurrent changes the spatial distribution of the longitudinal and transverse components of \mathbf{M} so as to minimize the free energy. That is, they give rise to an equilibrium distribution of the longitudinal magnetization in the upfield region by tipping \mathbf{M} by an angle $\beta \gg 104^\circ$ in the downfield region (where the fields are weaker). The magnetization consequently splits into two magnetic domains separated by a thin ($\sim 10^{-2}$ cm) domain boundary; \mathbf{M} is at rest in the upfield domain but precesses at an angle of $\sim 104^\circ$ relative to \mathbf{H} in the downfield (dynamic magnetic) domain. The dipole frequency shift (1) cancels the magnetic field gradient inside the dynamic magnetic domain (DMD), and the tipping angle β inside the DMD is given by

$$\gamma \nabla H x = -\delta \omega(\beta), \quad (2)$$

where x is the distance to the domain boundary. The proportion of the chamber filled by the domains is determined by

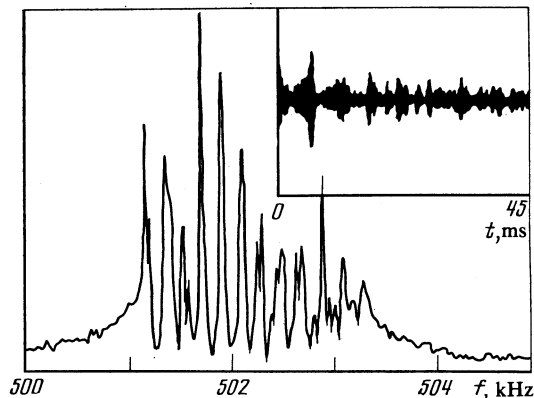


FIG. 5. Envelope and Fourier transform of the induction signal in an experimental chamber containing a stack of lavsan films ($P = 29.3$ bar, $H = 154$ Oe, $\nabla H = 1.5$ Oe/cm).

the initial tipping angle β_0 and by the magnetic relaxation processes. In the experiments the ^3He -filled chamber was connected by a channel to other parts of the chamber that were not exposed to the rf field of the NMR coils. In order to generate a DMD with a uniform precession under these conditions, special spin-current traps were needed to block the influx of the longitudinal magnetization from other parts of the chamber into the DMD. We verified this by carrying out experiments using chamber No. 2. We expected that a gradient magnetic field would give rise to a dynamic domain with a precessing magnetization, and that this domain would be localized within the sensitive region of weaker magnetic field. Figure 6 shows some NMR signal traces from ^3He -B recorded from coils 2 and 3 in chamber No. 2; the field gradients 0.1 Oe/cm were equal but oppositely directed in the two coils. The signal from the weak-field coil lasted for ~ 200 ms; under the same conditions, the NMR signals for normal-phase ^3He were identical for the two coils and decayed during ~ 10 ms. The field gradient thus changed the spatial distribution of the precessing magnetization and produced a DMD with a spatially uniform precession in the downfield region. This DMD was responsible for the slowly decaying signal.

We were able to analyze the time behavior of the DMD by using the two receiving coils in chamber No. 2. We first note that the conditions under which the DMD formed depended on the direction of the magnetic field gradient. The channel joining the ^3He in the experimental cell to the unexcited ^3He elsewhere in the chamber was located near coil 3. Consequently, when the field increased from coil 3 to coil 2 (so that the DMD formed near coil 3), the spin supercurrent flowed through the channel and carried the longitudinal magnetization of the ^3He from the rest of the chamber (where H was weaker) into the experimental cell. This explains why the SDS shown in Fig. 6b is shorter than is Fig. 6a. The difference between the durations of the SDS's for oppositely directed gradients increases abruptly with $|\nabla H|$, and this may prove useful in future studies of the kinematics of spin supercurrents in narrow channels. The field gradient in the subsequent studies was chosen so that the DMD formed in the sensitive region of coil 2.

The length of the DMD depends on the relaxation pro-

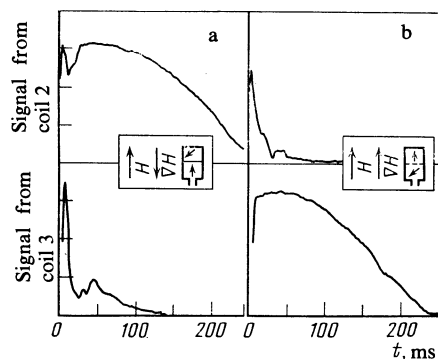


FIG. 6. Induction signal intensity from coils 2 and 3 for several magnetic field gradients; $T = 0.63T_c$, $P = 29.3$ bar, $H = 142$ Oe, $|\nabla H| = 0.1$ Oe/cm.

cesses that accompany domain formation and on the initial tipping angle β_0 . If we neglect the energy dissipation during DMD formation, geometric estimates yield

$$l = \frac{4}{5} l_0 (1 - \cos \beta_0), \quad (3)$$

for the length of the DMD in a cell which is closed off by walls parallel to the field; here l_0 is the total length of the NMR cell. Because of dissipation, the actual length is of course less. The familiar "bulk" mechanism of relaxation in superfluid ^3He involves collisions among excited quasiparticles and is effective only when the local precession frequency ω differs from ω_L . "Bulk" relaxation quickly restores β to 104° after an rf tipping pulse with $\beta_0 > 104^\circ$ is applied, and does not occur if β_0 is less than 104° . However, the spin supercurrents (which dissipate no energy) also shift ω relative to ω_L by transporting the transverse component of the magnetization in the nonuniform magnetic field. As a result, bulk relaxation may occur while the DMD is forming; this is clearly the reason why no DMD's can be observed for small initial angles $\beta_0 \lesssim 30^\circ$. A stable DMD forms for large β_0 .

Figure 7 shows some typical traces of the NMR signal induced in coils 2 and 3 for several values of β_0 . Unfortunately, the geometry of chamber No. 2 was such that we were unable to calibrate β_0 relative to the corresponding value for normal-phase ^3He , because the texture in the order parameter \mathbf{n} produced a nonlinear transient during the rf excitation pulse. Here we will concentrate on the properties of the NMR signal and defer the discussion of the nonlinear transient to the next section.

After a relatively weak rf excitation pulse was applied, a domain boundary formed in the narrow region where the

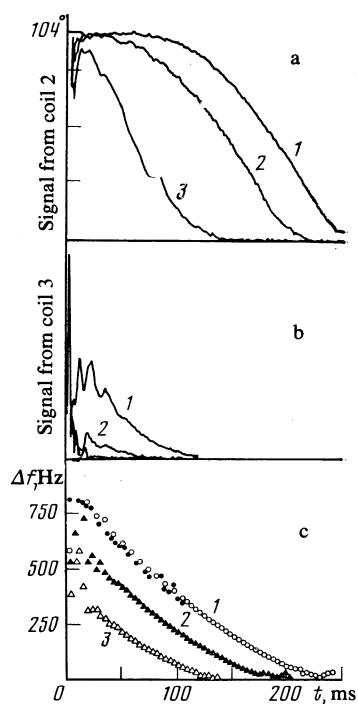


FIG. 7. Signal intensity from coils 2 and 3 and the frequency shift Δf as a function of time for several initial tipping angles. The circles and points show $\Delta f(t)$ for the signals from coils 2 and 3, respectively; $T = 0.6T_c$.

sensitive regions of coils 2 and 3 overlapped; however, the boundary formed in the sensitive region of coil 3 after the application of an rf pulse of moderate or high power. Since in all cases the DMD completely filled the entire sensitive region of coil 2, it is easy to estimate β in the DMD as a function of the NMR signal intensity I . As anticipated, I was the same as for the signal recorded from the normal phase of ^3He (with $\beta_0 = 104^\circ$) after correction for the magnetic susceptibility of $^3\text{He-B}$ at $T = 0.6T_c$. As time passes, the dissipation of the Zeeman energy (cf. below) causes the DMD to shrink and the domain boundary moves, as is clearly seen from Fig. 7. During the first 70 ms after the application of an intense rf pulse (curve 1), the moving boundary remains outside the sensitive region of coil 2, so that the NMR signal recorded from coil 2 is constant; however, the NMR signal from coil 3 drops due to the shrinkage of the DMD in its sensitive region. The receding boundary then enters the sensitive region of coil 2, and by $t = 100$ ms the signal intensity from coil 2 has dropped to roughly the same level as for coil 3; this occurs when the domain wall is exactly midway between the coils (in the narrow overlap region). The boundary then leaves coil 3 and moves continuously through the sensitive region of coil 2.

The signals are shifted in time for small β_0 , because the initial dimensions of the dynamical magnetic domain are smaller. The qualitative behavior of the NMR signal frequency thus supports our model description of the relaxation (shrinkage) of the DMD. However, it is better to extract quantitative information about the position of the domain boundary from the frequency characteristic of the slowly decaying signal. According to Fomin's theory,^{6,7} the precession frequency ω of the magnetization is equal to the Larmor frequency ω_L at the boundary between the two domains. Since the spatial distribution of the magnetic field is known, the position of the boundary can be deduced from the frequency of the SDS. As the boundary moves, ω should depend on the velocity of the boundary and the distribution of the magnetic field. The magnetic field gradient for the situation shown in Fig. 7 corresponded to a linear change of ≈ 1000 Hz in the Larmor precession frequency over the diameter of the chamber. Figure 7c shows the change Δf in the SDS frequency produced under the same conditions as for the signal traces 1–3 recorded from coil 2 (Fig. 7). The frequency of the SDS induced in coil 3 by signal 1 is also shown. The frequencies of signal 1 are seen to coincide for both coils, which confirms that both signals were produced by a single DMD. We can deduce the time dependence of the NMR signal from data on the time dependence $\Delta f(t)$ of the change in the SDS frequency, since $|\nabla H|$ and the spatial distribution of the sensitivity of coil 2 are known; this dependence can then be compared with the experimental result. Here we must also know the Larmor frequency corresponding to the minimum magnetic field inside the experimental chamber. The dependence deduced by the above method is found to agree closely with the experimental result. Figure 7 does not show the SDS intensity reconstructed at the signal frequency, because it is virtually identical to the experimental dependence for times $40 \leq t \leq 200$ ms. The amplitude and frequency characteristics of the SDS thus agree quantitatively

with the theoretical predictions. Once the DMD has relaxed, the signal frequency decreases more slowly or may even start to increase, possibly because the domain wall interacts with the wall of the experimental chamber (this may become important if the thickness of the DMD and chamber walls are comparable). According to the theory, there is no signal from the second domain (located at higher magnetic fields) because \mathbf{M} is parallel to \mathbf{H} . However, spatial dephasing of the precessing magnetization could also suppress the NMR signal. In order to explore this further, we measured the signal intensity from coil 3 after a single weak rf pulse was applied; we then measured the intensity after an identical rf pulse was applied while the SDS was observed in coil 2. The signals were identical in both cases, which implies that the longitudinal magnetization was in equilibrium in the second (static) domain.

INFLUENCE OF TEXTURE ON DMD FORMATION

Before discussing the remaining experimental results, we will examine how the external conditions and the texture of the order parameter vector \mathbf{n} in $^3\text{He-B}$ influence the properties of the SDS and the formation of the dynamic magnetic domain. The texture and its effects on the NMR spectrum were studied in detail in Ref. 10 for cylindrical chambers with various magnetic field orientations. The results there imply that a homogeneous texture \mathbf{n} should form in chamber No. 1, whose experimental cell was cylindrical with axis normal to the magnetic field. However, singular configurations that distort the texture may form on the sides of the chamber, and this could be responsible for the poor reproducibility of the SDS pulseform in chamber No. 1 at zero field gradient. However, a weak gradient field sufficed to stabilize the SDS by stabilizing the spatial distribution of the spin supercurrents.

The axis of the cylindrical experimental cell in chamber No. 2 was parallel to \mathbf{H} ; in this case, the results in Ref. 10 predict a conically expanding texture of \mathbf{n} with $\theta \sim 60^\circ$ and $\varphi \approx 63^\circ$ near the chamber walls (here θ and φ are the polar and azimuthal angles that determine the orientation of \mathbf{n} in a spherical coordinate system with polar axis parallel to \mathbf{H} ; φ is measured from the tangent to the surface of the cylinder). The vector \mathbf{n} rotates smoothly along \mathbf{H} with a constant azimuthal velocity as we move away from the walls. Since the NMR frequency in $^3\text{He-B}$ depends on the orientation of \mathbf{n} , the frequency of the continuous-wave (cw) NMR signal is upshifted by ~ 10 kHz in accordance with the distribution of \mathbf{n} in the chamber. The textural effects on the cw NMR frequency are particularly pronounced at low temperatures, for which the diameter of the region in which \mathbf{n} is rotated becomes comparable to the diameter of the chamber. The processes in $^3\text{He-B}$ following deflection of \mathbf{n} away from \mathbf{H} by and NMR excitation pulse were studied in Ref. 11, where it was shown that a sufficiently intense rf pulse should make \mathbf{n} precess near the wall, and the precession should correspond to a free precession of the magnetization. The spectra of the rf pulses in our experiment contained the cw NMR spectrum as a proper subinterval. However, we observed (as in Ref. 11) that the spin system in $^3\text{He-B}$ was excited more effectively at low temperatures when the rf pulse frequency ω was ~ 10

kHz higher than the Larmor frequency ω_L . When we varied ω within the interval $|\omega - \omega_L| \leq 50$ kHz (equal to the spectral width of the rf pulse) in the presence of a gradient magnetic field, we found that the only effect was to produce quantitative changes in the signals from coils 2 and 3 which could be eliminated by increasing the rf power.

An abrupt change in the form and properties of the SDS was detected during one of the demagnetizing cycles. In this cycle the ^3He superfluid transition occurred at 150 Oe, and an ordinary SDS was observed at $T \sim 0.4T_c$ and $P = 15$ bar. We then decreased H to 70 Oe and found that the SDS signal was very short, which we attributed to the large nonuniform NMR shift caused by the texture. We then applied a series of rf pulses separated by a small delay ~ 1 sec, and observed that the signal became irregular (a jumble of peaks and valleys). After H was increased to 150 and 250 Oe, the signal became much shorter than it was initially and remained irregular. The Fourier transform of the SDS revealed two nearly equal frequencies in the spectrum. The usual form of the SDS signal for chamber No. 2 was restored during the next cycle (each cycle consisted of heating the helium to the normal phase, followed by cooling to the superfluid $^3\text{He-B}$ phase).

We recall that Ref. 10 studied the texture in a cylindrical chamber with axis parallel to the field. According to those experimental results, the conically expanding texture is not the only possible one—a texture \mathbf{n} with two singular lines along the sides of the cylinder (parallel to \mathbf{H}) may remain metastable. The interaction of the spin supercurrents with this metastable texture on the chamber wall could be responsible for the unusual form of the SDS signal. We note that this unconventional SDS signal was observed only once in the entire series of experiments.

Our experiments imply that the following three basic conditions must be met in order for well-formed SDS signals to be observed. 1) A constant magnetic field gradient must exist in the chamber (i.e., the field must vary linearly), and the experimental chamber must be bounded in the direction opposite to the gradient. 2) The texture \mathbf{n} must be spatially uniform near the wall. 3) The rf excitation pulse must be short and its spectrum must completely contain the spectrum of the cw NMR signal. The latter requirement implies that rather intense rf pulse must be used; unfortunately, this means setting up a thermal pulse in the coils. The latter must therefore be thermally isolated from the experimental chamber in order to avoid heating the ^3He during the SDS.

RELAXATION OF THE DYNAMIC MAGNETIC DOMAIN

The properties of the DMD described in the preceding section can be exploited to measure the magnetic relaxation processes in $^3\text{He-B}$. According to the relaxation theory in Refs. 6 and 7, two mechanisms of Zeeman energy dissipation are responsible for the shrinkage of the DMD. These are the bulk relaxation mechanism proposed for superfluid ^3He by Leggett and Takagi,¹² and spin diffusion (a surface effect) across the boundary separating the static and dynamic magnetic domains. It will therefore be helpful in comparing and differentiating between these mechanisms to use and experi-

mental chamber (e.g., chamber No. 2) with a constant cross section normal to the magnetic field. The internal mechanism dissipates the Zeeman energy at a rate proportional to the frequency difference between the precession and Larmor frequencies: $dE/dt \propto \delta\omega$. Since $\delta\omega$ varies linearly with distance from the domain boundary when a constant-gradient field is applied (2), an integration over the volume of the DMD gives the result

$$\frac{dE}{dt} \propto (\Delta\omega)^2 l \quad (4)$$

for the energy dissipation as a function of the length l of the DMD. Here $\Delta\omega = \omega - \omega_0$, where $\omega_0 = \gamma H_{\min}$ is the minimum Larmor frequency (H_{\min} is the minimum magnetic field inside the chamber). Since the tipping angle β is $\sim 104^\circ$ inside and 0° outside the DMD, the dissipation dE/dt displaces the domain boundary,

$$v \propto dE/dt. \quad (5)$$

On the other hand, spin diffusion across the boundary is associated with an energy dissipation^{6,7}

$$\frac{dE}{dt} \sim D \left(\frac{\gamma^2 H \nabla H}{c^2} \right)^{1/2}, \quad (6)$$

where c is the velocity of the spin waves and D is the spin diffusion coefficient. The velocity of the boundary was found from the change in the SDS frequency in the experiments: $\dot{\omega} = v\gamma\nabla H$; it will therefore be helpful to use the numerical coefficients given in Refs. 6 and 7 to express the dissipation in terms of $\dot{\omega}$. We find that

$$\dot{\omega} = 0.88 \frac{D}{c^{2/3}} (\nabla\omega)^{1/3} \omega^{1/6} - \frac{1}{4} \tilde{\tau}_{LT} (\Delta\omega)^3, \quad (7)$$

where $\nabla\omega = \gamma\nabla H$, and the bulk relaxation time $\tilde{\tau}_{LT}$ was measured experimentally in Ref. 13. The first (diffusion) term thus leads to a linear time dependence of the SDS frequency. The second (bulk) term becomes much less important as l decreases. The experimental dependence $\omega(t)$ in a constant-gradient field usually contain a well-defined linear section which corresponds to diffusion-dominated relaxation. Bulk relaxation becomes important only for large $|\nabla H|$ and l . Figure 8 shows the frequency difference $f(t) - f(0)$ of the SDS recorded at $T = 0.69T_c$, $P = 20$ bar for $|\nabla H| = 2.5$ Oe/cm; $f(t)$ clearly approaches a straight line. Toward the end of the relaxation process, $f(t)$ becomes nonlinear, possibly (as noted above) due to interaction of the domain boundary with the wall of the experimental chamber. In order to quantitatively compare the theory with experiment, we used a computer to choose the values of $\tilde{\tau}_{LT}$ and $D/c^{2/3}$ for which Eq. (7) best approximates the experimental points. The results are shown by the solid curve in Fig. 8. We were unable to determine the relaxation time $\tilde{\tau}_{LT}$ accurately because of the considerable error in ω_0 . However, $D/c^{2/3}$ was deduced from the slope of $f(t)$ toward the end of the SDS signal and was insensitive to variations in ω_0 and $\tilde{\tau}_{LT}$. This thus provides a way to measure the rate of spin diffusion relaxation and hence deduce the constant $D/c^{2/3}$ (assuming the correctness of the theory of spin diffusion relaxation). The error increases substantially if the spin diffusion relaxation rate is

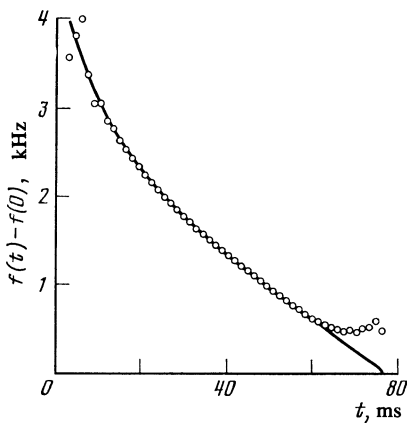


FIG. 8. The symbols \circ show the time dependence of the frequency of the SDS ($T = 0.69T_c$, $P = 20$ bar, $|\nabla H| = 2.5$ Oe/cm); the solid curve gives the theoretical dependence Eq. (7).

deduced from the dependence on the magnetic field gradient. According to Eq. (7), $\dot{\omega} \propto (\nabla\omega)^{4/3}$ if the bulk relaxation is neglected.

Figure 3 in Ref. 5 shows $f(t)$ for several magnetic field gradients. Figure 9 plots the slopes $df(t)/dt$ on the linear portions of the curves as a function of $|\nabla H|$; we see that the dependence $(\dot{\omega})^{3/4} = \text{const}$ closely approximates the experimental points. This result supports the correctness of the theory of DMD relaxation and provides a more accurate way of assessing the relative importance of spin diffusion across the domain boundary (this information in turn can be used to deduce the rate of bulk relaxation from the experimental data). We will analyze bulk and spin-diffusion relaxation more systematically in a subsequent paper; here we merely state that the above theory gives results in good agreement with experiment, both with regard to DMD formation and with regard to the relaxation processes.

Finally, Fig. 10 shows the temperature dependence of the rate of change of the SDS frequency [divided by $(\nabla\omega)^{4/3}$] due to spin diffusion relaxation. The right-hand scale gives the values of $D/c^{2/3}$ deduced by Eq. (7) from the experimental data. The temperature dependence of $D/c^{2/3}$ for $T > 0.8T_c$ has the same qualitative form as for the spin-wave velocity. Further study is needed to understand why $D/c^{2/3}$ drops for $T < 0.6T_c$; the decrease could conceivably be due to an analog of the Leggett-Rice effect¹⁴ in normal ^3He , in which spin diffusion is retarded for $\omega\tau \gtrsim 1$.

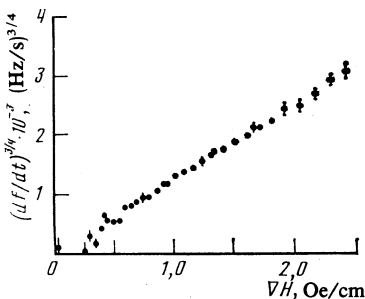


FIG. 9. The linear (diffusion) term in Eq. (7) as a function of the magnitude of the magnetic field gradient ($H = 154$ Oe, $T = 0.74T_c$, $P = 20$ bar).

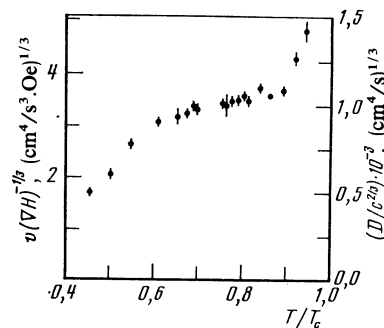


FIG. 10. Temperature dependence of the linear term in (7) [divided by $|\nabla H|^{1/3}$] for $P = 20$ bar, $H = 154$ Oe.

CONCLUSIONS

Our results imply that the transport of nuclear spin magnetization by the spin supercurrents dominates the behavior of the magnetization after a tipping rf pulse is applied to $^3\text{He-B}$ in a spatially varying magnetic field ($H = 10^{-4}$ – 100 Oe/cm). These currents carry the longitudinal component of the magnetization toward higher fields. Quantum effects generate an unusual macroscopic dynamic magnetic domain if the chamber containing the ^3He is closed off downfield (opposite to the gradient ∇H). The magnetization vector in $^3\text{He-B}$ precesses uniformly even though $|\nabla H|$ is non-zero.

Magnetization transport by spin supercurrents and the formation of dynamic magnetic domains must be treated in order to interpret the results of pulsed and cw NMR experiments. For example, pulsed NMR was employed in Refs. 1 and 3 to study the recovery of the longitudinal magnetization in $^3\text{He-B}$, and the recovery rate was found to be proportional to $|\nabla H|$. We can interpret this finding as follows. The recovery process in the sensitive region of the rf coil was not local but instead involved a transport of longitudinal magnetization from the downfield regions of the chamber; moreover, the magnetic field gradient determined the magnitude of the spin supercurrent.

According to the experiments discussed above, the relaxation of the magnetization in $^3\text{He-B}$ can be attributed entirely to shrinkage of the DMD caused by bulk relaxation and spin diffusion across the domain wall. The nature of the relaxation processes that occur while the DMD is forming remains to be determined; at the very least, both bulk and spin diffusion relaxation should occur during the formation stage. Observations of DMD relaxation will make it possible for the first time to measure the spin diffusion in superfluid ^3He .

We note in closing that the transport of the magnetization by the spin supercurrents also plays a decisive role in the behavior of the magnetization precession in $^3\text{He-A}$. Here, however, the spin currents destabilize the precession⁹ because of the specific nature of the dependence of the free energy on the tipping angle.

We thank I. A. Fomin for a pleasant and fruitful collaboration, and S. M. Elagin and V. I. Kirillov for technical assistance.

¹⁾Institute of Experimental Physics, Slovak Academy of Science, Košice, Czechoslovakia.

- ¹L. R. Corruccini and D. D. Osheroff, *Phys. Rev. Lett.* **34**, 564 (1975).
²W. F. Brinkman and H. Smith, *Phys. Lett.* **53A**, 43 (1975).
³L. R. Corruccini and D. D. Osheroff, *Phys. Rev. B* **17**, 126 (1978).
⁴R. W. Giannetta, E. N. Smith, and D. M. Lee, *J. Low Temp. Phys.* **45**, 295 (1981).
⁵A. S. Borovik-Romanov, Yu. M. Bun'kov, V. V. Dmitriev, and Yu. M. Mukharskii, *Pis'ma Zh. Eksp. Teor. Fiz.* **40**, 256 (1984) [*JETP Lett.* **40**, 1033 (1984)].
⁶I. A. Fomin, *Pis'ma Zh. Eksp. Teor. Fiz.* **40**, 260 (1984) [*JETP Lett.* **40**, 1037 (1984)].
⁷I. A. Fomin, *Zh. Eksp. Teor. Fiz.* **88**, 2039 (1985) [*Sov. Phys. JETP* **61**, (1985)] (next article, this issue).
⁸A. S. Borovik-Romanov, Yu. M. Bun'kov, V. V. Dmitriev, Yu. M. Muk-

- harskii, and G. K. Tvalashvili, *Prib. Tekh. Eksp.*, No. 3, 185 (1985).
⁹Yu. M. Bun'kov, V. V. Dmitriev, and Yu. M. Mukharskii, *Zh. Eksp. Teor. Fiz.* **88**, 1218 (1985) [*Sov. Phys. JETP* **61**, (1985)].
¹⁰Yu. M. Bun'kov, P. J. Hakonen, and M. Krusius, in: *Proc. Symp. "Quantum Fluids and Solids,"* AIP Conf. Proc., No. 103, New York (1983), pp. 194-209.
¹¹A. S. Borovik-Romanov, Yu. M. Bun'kov, V. V. Dmitriev, and Yu. M. Mukharskii, *Pis'ma Zh. Eksp. Teor. Fiz.* **37**, 600 (1983) [*JETP Lett.* **37**, 716 (1983)].
¹²A. Leggett and S. Takagi, *Phys. Rev. Lett.* **34**, 1424 (1975).
¹³G. Eska, K. Neumaier, W. Shoepe, K. Uhlig, and W. Wiedeman, *Phys. Lett.* **87A**, 311 (1980).
¹⁴L. R. Corruccini, D. D. Osheroff, D. M. Lee, and R. C. Richardson, *J. Low Temp. Phys.* **8**, 229 (1972).

Translated by A. Mason